PTEP

Structure of the Ω baryon and the kaon cloud

Yu-Son Jun[1], Hyun-Chul Kim[1,2,⋆], June-Young Kim[3], and Jung-Min Suh[1]

[1]*Department of Physics, Inha University, Incheon 22212, Republic of Korea*
[2]*School of Physics, Korea Institute for Advanced Study (KIAS), Seoul 02455, Republic of Korea*
[3]*Institut für Theoretische Physik II, Ruhr-Universität Bochum, D-44780 Bochum, Germany*
⋆E-mail: hchkim@inha.ac.kr

....
We investigate the effects of the kaon cloud on the electromagnetic and axial-vector form factors of the Ω^- baryon within the framework of the chiral quark-soliton model. We first derive the profile function of the chiral soliton in such a way that the kaon Yukawa tail is properly produced self-consistently. Then, we compute the electromagnetic form factors of the Ω^- baryon. The results for the electromagnetic form factors are compared with the lattice data. We find that the results with the kaon tail are in better agreement with the lattice data than those obtained with the pion tail. We also study the axial-vector form factors of the Ω^- baryon, examining the effects of the kaon cloud.
....
Subject Index   D32

1. Introduction

The lowest-lying Ω baryon is the strangest particle among all hadrons. It is also a member of the baryon decuplet and was the last of the lowest-lying decuplet baryons to be found [1]. The excited state $\Omega(2250)^-$ was only found after another two decades [2–4]. More interestingly, the first excited state $\Omega(2012)^-$ was found only very recently [5,6]. The Particle Data Group (PDG) summarized the existence of the four excited states [7] only. This indicates that the Ω baryons have been least studied among hyperons. A very recent measurement of the correlation function for the proton (*p*)–Ω interaction has triggered interest in these Ω baryons [8]. It reveals that the *p*–Ω potential is attractive even though the relative distance between *p* and Ω goes to zero, which implies the possible existence of the *p*–Ω bound state [9]. Meanwhile, the electromagnetic (EM) form factors and axial charges of the ground-state Ω baryon have been computed in lattice quantum chromodynamics (QCD) [10,11].

The nucleon has been known to be dressed by the pion cloud in various contexts [12–22]. The pion cloud can be qualitatively understood as $q\bar{q}$ excitations within the framework of QCD [19] or as the pion loop in effective field theory [21]. The large-N_c (the number of colors) limit of QCD still provides a lucid point of view of the pion cloud of the nucleon [23]. Nucleons emerge as states of N_c valence quarks bound by the pion mean field, which is produced by the presence of the N_c valence quarks. This pion mean field can be regarded as the pion cloud. In the Skyrme model with the finite pion mass included, which is the simplest case of the pion mean-field approach, the expectation value of the pion field in a nucleon shows asymptotic behavior: $\langle \pi^a(r) \rangle \sim e^{-m_\pi r} x^i r^{-2} \langle \sigma_i \tau^a \rangle$ [18]. A more realistic pion mean-field approach such as the chiral quark-soliton model (χQSM) [24,25] also provides the pion cloud from Dirac-sea polarization or the Dirac-sea continuum [26,27].

On the other hand, the Ω baryon is not coupled to the pion, since it is an isosinglet baryon and consists only of strange valence quarks. However, the SU(3) baryons are constructed in the χQSM by embedding the SU(2) soliton into flavor SU(3) space, so all the lowest-lying baryons in the model have a pion tail [25,28,29] in common. While this is theoretically consistent, it does not reflect the phenomenology properly. Since the hyperons contain the strange quark, the kaon cloud should naturally come into play in describing their structure. Even in the case of the nucleon, the kaon cloud provides certain effects when the strangeness in the nucleon is examined [30–34]. However, in any chiral solitonic approaches, it is impossible to consider both the pion and kaon clouds in a compatible manner. This means that one should choose either the pion cloud or the kaon one, depending on which observables of the hyperons are being investigated. For example, the electric form factors of the neutron or neutral hyperons are rather sensitive to meson tails. Fortunately, the Ω baryon contains three strange valence quarks and it is not coupled to the pions, so we can choose the kaon tail in place of the pion one. Of course, one may still raise a question about the contributions from the η and $\eta^{'}$ clouds, since these two pseudoscalar mesons also contain hidden strangeness, so that they can be coupled to the Ω baryon. The coupling between η and Ω is known to be rather small [35], so the effect of the η on the Ω baryon is also expected to be small. Since the mass of $\eta^{'}$ is much larger than the pseudoscalar meson octet, its effect should be suppressed. Thus, as long as we are only concerned with the Ω baryon, the present approach will still shed light on the effects of the kaon cloud or the kaon tail on the structure of the Ω baryon.

In the present work, we will investigate the EM and axial-vector structures of the Ω^- baryon considering the effects of the kaon cloud. We first review the kaon properties based on the effective chiral action and fix the relevant parameters such as the pion decay constant and the pion and kaon masses. We will then introduce the effective mass of the current strange quark in the Dirac Hamiltonian and solve the classical equation of motion, so that we are able to derive the profile function of the chiral soliton with the proper kaon tail. Then we will perform symmetry-conserving zero-mode quantization [36]. We will focus on examining the EM and axial-vector form factors of the Ω baryon, taking into account the $1/N_c$ rotational corrections on them. Since the effects of the explicit breaking of flavor SU(3) symmetry are rather small, we do not include them in the present work. Finally, we will compare the present results with those from lattice QCD and explicitly show that the kaon cloud plays an essential role in describing the Ω baryon.

The present paper is organized as follows: In Sect. 2, we start from the effective chiral action to study the properties of the kaon. Expanding the effective action by using the background field method, one can find the kaon propagator for which the pole yields the mass of the kaon and its residue becomes its decay constant. This process is similar to the usual renormalization of a particle. Then we proceed to the solitonic sector and derive the equation of motion, the solution of which leads to the meson mean field. The kaon cloud can be incorporated by using the corresponding quark mass inside the one-body Dirac Hamiltonian. The classical solution, which is identified as the classical mass of the Ω baryon, possesses a Yukawa tail with the proper kaon mass. This will play a key role in describing the EM and axial-vector form factors of Ω. In Sect. 3, we briefly recapitulate the formulae for the EM and axial-vector form factors. In Sect. 4, we present the numerical results and discuss them, comparing them with those from lattice QCD. Section 5 is devoted to the summary and conclusion of the present work. In the

appendices, we compile expressions for the EM and axial-vector form factors, derived from the χQSM.

2. Kaon properties and kaon cloud

The effective chiral action and its partition function in Euclidean space are given as

$$Z_{e} = \int \mathcal{D}\psi^{\dagger}\mathcal{D}\psi\mathcal{D}\pi^{a}\exp\left[\int d^{4}x\psi^{\dagger}iD(\pi^{a})\psi\right] = \int \mathcal{D}\pi^{a}\exp[-S_{e}], \tag{1}$$

where S_{eff} represents the effective chiral action expressed by

$$S_{e}[\pi] = -N_{c}\text{Tr} \ln (i\partial\!\!\!/ + i\hat{m} + iMU^{\gamma_5}(\pi^{a})). \tag{2}$$

Here, N_{c} is the number of colors. Tr denotes the functional trace over the space-time, spin space, and flavor space. M designates the dynamical quark mass. $\hat{m}$ is the matrix of the current quark masses:

$$\hat{m} = \begin{pmatrix} m_{\text{u}} & 0 & 0 \\ 0 & m_{\text{d}} & 0 \\ 0 & 0 & m_{\text{s}} \end{pmatrix}. \tag{3}$$

U^{γ_5} stands for the chiral field expressed by

$$U^{\gamma_5} = \frac{1 + \gamma_5}{2}U + \frac{1 - \gamma_5}{2}U^{\dagger} \tag{4}$$

with

$$U(x) = \exp\left[\frac{i}{f}\lambda^{a}\pi^{a}(x)\right]. \tag{5}$$

Here, f is introduced as a scale factor that makes the argument of Eq. (5) dimensionless. π^{a} represents the pseudo-Nambu–Goldstone fields expressed as

$$\lambda^{a}\pi^{a} = \begin{pmatrix} \frac{1}{\sqrt{2}}\pi^{0} + \frac{1}{\sqrt{6}}\eta & \pi^{+} & K^{+} \\ \pi^{-} & -\frac{1}{\sqrt{2}}\pi^{0} + \frac{1}{\sqrt{6}}\eta & K^{0} \\ K^{-} & \bar{K}^{0} & -\frac{2}{\sqrt{6}}\eta \end{pmatrix}. \tag{6}$$

2.1 Kaon properties

We first examine the meson properties based on the effective chiral action [26,37,38]. Introducing the meson source j^{a} explicitly, we write the generating functional as follows:

$$\mathcal{Z}[j] = \int \mathcal{D}\pi^{a}e^{-S_{e}+j\cdot\pi}, \tag{7}$$

which gives the mesonic two-point correlation function as

$$K^{ab}(x - y) = \left.\frac{\delta^{2}\ln\mathcal{Z}}{\delta j^{a}(x)\delta j^{b}(y)}\right|_{j=0}, \tag{8}$$

where $j \cdot \pi = \int d^{4}xj^{a}(x)\pi^{a}(x)$. Note that in the present model the mesons emerge as low-lying collective $\bar{\psi}\psi$ excitations. Using the background field method [39], one can decompose the mesonic field π^{a} into two parts:

$$\pi^{a}(x) = \pi_{c}^{a}(x) + \delta\pi^{a}(x), \tag{9}$$

where π^{a} is the solution of the classical equation of motion

$$\frac{\delta S}{\delta\pi^{a}(x)} = 0, \tag{10}$$

which is just the same as the classical value of π^a:

$$\pi_c^a(x) := \langle \pi^a \rangle = \left. \frac{\delta \ln \mathcal{Z}}{\delta j^a(x)} \right|_{j=0}. \tag{11}$$

Then, the generating functional can be written as

$$\ln \mathcal{Z} = -S_{e}[\pi_c^a] + j \cdot \pi_c - \frac{1}{2} \text{Tr} \ln \left[\frac{\delta^2 S}{\delta \pi \delta \pi} \right] + \frac{1}{2} j \left[\frac{\delta^2 S}{\delta \pi \delta \pi} \right]^{-1} j, \tag{12}$$

where the last term is shorthand notation for

$$j \left[\frac{\delta^2 S}{\delta \pi \delta \pi} \right]^{-1} j = \int d^4x d^4y \, j^a(x) \frac{\delta^2 S}{\delta \pi^a(x) \delta \pi^b(y)} j^b(y). \tag{13}$$

Note that the first term of Eq. (12) is the effective action that is proportional to N_c as shown in Eq. (2). The third term is known to be the one meson-loop contribution, which is proportional to $1/N_c$. In the large-N_c limit, this is suppressed. As shown in Eq. (12), the inverse of the meson propagator is expressed by

$$(K_\pi^{ab})^{-1} = \left. \frac{\delta^2 S_{e}}{\delta \pi^a(x) \delta \pi^b(y)} \right|_{\pi_c}. \tag{14}$$

Expanding S_{eff} with respect to the meson fields, we obtain the inverse of the pion and kaon propagators in momentum space as follows [30,40]:

$$\frac{1}{Z_\pi(p^2)} \frac{1}{\delta^4(0)} \left. \frac{\delta^2 S_{e}}{\delta \pi^a(p) \pi^a(-p)} \right|_{p^2=-m_\pi^2} = (p^2 + m_\pi^2) \Big|_{p^2=-m_\pi^2}, \quad a = 1, 2, 3,$$

$$\frac{1}{Z_K(p^2)} \frac{1}{\delta^4(0)} \left. \frac{\delta^2 S_{e}}{\delta \pi^a(p) \pi^a(-p)} \right|_{p^2=-m_K^2} = (p^2 + m_K^2) \Big|_{p^2=-m_K^2}, \quad a = 4, \ldots, 7. \tag{15}$$

The poles of the meson propagators yield the masses of the pion and kaon:

$$m_\pi^2 = \frac{m_0 I_1(M, m_0)}{Z_\pi(p^2 = -m_\pi^2)} M = (139 \,\text{MeV})^2,$$

$$m_K^2 = \frac{m_0 I_1(M, m_0) + m_s I_1(M, m_s)}{2 Z_K(p^2 = -m_K^2)} M + (m_0 - m_s)^2 = (496 \,\text{MeV})^2, \tag{16}$$

where

$$I_1(M, m_0) = 4N_c \int \frac{d^4k}{(2\pi)^4} \frac{M^2}{k^2 + (M + m_0)^2}. \tag{17}$$

m_0 denotes the average current quark mass, i.e., $m_0 = (m_u + m_d)/2$. Z_π and Z_K stand for the renormalization constants for the pion and kaon wavefunctions, given as

$$Z_\pi(p^2) = 2N_c \int \frac{d^4k}{(2\pi)^4} \frac{M^2}{k^2 + (M + m_0)^2} \frac{M^2}{(k + p)^2 + (M + m_0)^2},$$

$$Z_K(p^2) = 2N_c \int \frac{d^4k}{(2\pi)^4} \frac{M^2}{k^2 + (M + m_0)^2} \frac{M^2}{(k + p)^2 + (M + m_s)^2}. \tag{18}$$

Since I_1 and the renormalization constants are divergent, we use proper-time regularizations in this work [30,40].

The meson decay constants f_π and f_K are defined as the transition from the meson state to the vacuum through the axial-vector current

$$\langle 0 | A_\mu^a(x) | \phi^b(q) \rangle = i q_\mu f_\phi e^{-iq \cdot x} \delta^{ab}, \tag{19}$$

where ϕ^a denotes generically the pion or the kaon. The axial-vector current is given by $A_\mu^a(x) = i\psi^\dagger(x) \gamma_\mu \gamma_5 \frac{\lambda^a}{2} \psi(x)$ in Euclidean space. After some lengthy calculations [26,30,40], we obtain the

pion and kaon decay constants:

$$f_\phi(p) = \frac{\sqrt{2Z_\phi(p)}}{M}. \tag{20}$$

Using Eqs. (16) and (20), we obtain the Gell-Mann–Oakes–Renner relation:

$$f_\pi^2 m_\pi^2 = -m_0 i \langle \psi^\dagger(0)\psi(0)\rangle_0, \tag{21}$$

where the quark condensate $i\langle \psi^\dagger(0)\psi(0)\rangle_0$ is given by

$$\langle i\psi^\dagger(0)\psi(0)\rangle_0 = -2\frac{I_1(M, m_0)}{M}. \tag{22}$$

The cutoff parameter Λ and the average current quark mass m_0 are fixed by the pion decay constant and the pion mass, respectively. The dynamical quark mass M is considered to be a free parameter. We take its value to be $M = 420$ MeV, with which baryonic properties have been well reproduced [26]. The strange current quark mass $m_s = 150$ MeV yields the kaon mass $m_K = 496$ MeV. In the present work, we do not consider the effects of explicit flavor SU(3) symmetry breaking, since they are marginal.

2.2 Kaon cloud

Once the parameters of the model are fixed in the mesonic sector, we can proceed to the baryonic sector. The effective chiral action S_{eff} in Eq. (2) can be expressed in terms of the one-body Dirac Hamiltonian

$$H = \gamma_4 \gamma_k \partial_k + M\gamma_4 U^{\gamma_5} + m_0 \gamma_4, \tag{23}$$

for which the eigenenergies and eigenstates of a quark are given by $H|n\rangle = E_n|n\rangle$. Having computed the nucleon correlation function (see Refs. [25,26] for details), we obtain the classical mass as

$$M_{\text{cl}} = N_c E_{\text{val}}[\pi^a] + E_{\text{sea}}[\pi^a], \tag{24}$$

where E_{val} denotes the energy given by the N_c valence quarks in the lowest upper Dirac level, which yields a state with baryon number one. E_{sea} stands for the energy that is required for the pion mean field to be created. This is just the sum of the energies of the quarks in the lower Dirac continuum. Note that both the energies E_{val} and E_{sea} are given as functionals of the pion field. Using the classical equation of motion for the pion mean field, we can minimize the energy of the classical nucleon or the chiral soliton. The final solution of the pion mean field is expressed as

$$\pi_c^a(\boldsymbol{x}) = n^a P(r), \tag{25}$$

where $P(r)$ designates the profile function of the chiral soliton and n^a is a normal vector in isospin space, defined as $n^a = x^a/\|\boldsymbol{x}\|$. We embed this stationary solution into SU(3) as follows:

$$U(\boldsymbol{x}) := \begin{pmatrix} \exp[i\boldsymbol{n}\cdot\boldsymbol{\tau}P(r)] & 0 \\ 0 & 1 \end{pmatrix}. \tag{26}$$

m_0 in Eq. (23) plays an essential role in producing the correct proper Yukawa-type asymptotic behavior of the profile function:

$$P(r) = \alpha \exp(-\overline{m}_\pi r)\frac{1 + \overline{m}_\pi r}{r^2}, \tag{27}$$

where α denotes a constant that governs the strength of the profile function and $\overline{m}_\pi$ represents the generic meson mass that produces the required meson tail. For instance, $\overline{m}_\pi = m_\pi = 139$ MeV corresponds to the pion cloud whereas $\overline{m}_\pi = m_K = 496$ MeV produces the proper kaon

cloud. As mentioned in the introduction, however, the Ω is not coupled to the pion but to the kaon. Unfortunately, no chiral solitonic approach can take the pion and kaon mean fields into account separately. Since we quantize the SU(3) soliton in Eq. (26) by rotating it slowly in the coordinate and flavor spaces, both the pion and kaon fields have the same pion tail. To investigate the properties of the Ω^- baryon, it is natural to consider only the kaon mean field. Of course, this is a rather phenomenological approach but is necessary to describe Ω^- more physically. Thus, we increase the value of m_0 such that the proper kaon cloud is produced, i.e., $\overline{m}_\pi = m_K = 496$ MeV in Eq. (27). Once we obtain the profile function with the kaon cloud, we can compute various properties of Ω^-. As will be shown soon, the chiral soliton with the kaon cloud describes the EM and axial-vector form factors far better than that with the pion cloud, when the results are compared with those from lattice QCD. Since we are mainly interested in the effects of the kaon cloud, we will compute all the observables, imposing flavor SU(3) symmetry without its explicit breaking considered.

One may argue that the effects of flavor SU(3) symmetry breaking are too large to be ignored as shown in the Skyrme model with the bound-state approach [41] and Yabu–Ando's approach [42]. In fact, Yabu–Ando's approach has been examined within the present framework [40], where they have computed the mass spectrum of the hyperons. The results showed clearly that the higher-order corrections ($\mathcal{O}(m_s^3)$) are negligible, since they are rather similar to those obtained by the perturbative approach. This indicates that the effects of flavor SU(3) symmetry breaking are rather small. In fact, we found that these effects turned out to be at most 10% for almost all baryonic observables [26]. So, we will only consider the flavor SU(3) symmetric case.

3. Electromagnetic and axial-vector form factors of the Ω^- baryon

We first compute the EM form factors of the Ω^- baryon. Since the general formalism was presented in Ref. [43] in detail, we briefly recapitulate it. The matrix element of the EM current in Euclidean space is defined as

$$J^\mu(x) := i\psi^\dagger(x)\gamma^\mu \hat{\mathcal{Q}}\psi(x), \tag{28}$$

where $\psi(x)$ denotes the quark field. The charge operator of the quarks $\hat{\mathcal{Q}}$ is written in terms of the flavor SU(3) Gell-Mann matrices λ_3 and λ_8:

$$\hat{\mathcal{Q}} = \begin{pmatrix} \frac{2}{3} & 0 & 0 \\ 0 & -\frac{1}{3} & 0 \\ 0 & 0 & -\frac{1}{3} \end{pmatrix} = \frac{1}{2}\left(\lambda_3 + \frac{1}{\sqrt{3}}\lambda_8\right). \tag{29}$$

The matrix elements of the EM current between the Ω^- baryons can be parametrized by four form factors F_i ($i = 1, \ldots, 4$) as follows:

$$\langle \Omega^-(p', s)|J^\mu(0)|\Omega^-(p, s)\rangle = -\overline{u}^\alpha(p', s)\left[\gamma^\mu \left\{F_1(q^2)\eta_{\alpha\beta} + F_3(q^2)\frac{q_\alpha q_\beta}{4M_\Omega^2}\right\}\right.$$
$$\left. + i\frac{\sigma^{\mu\nu}q_\nu}{2M_\Omega}\left\{F_2(q^2)\eta_{\alpha\beta} + F_4(q^2)\frac{q_\alpha q_\beta}{4M_\Omega^2}\right\}\right]u^\beta(p, s), \tag{30}$$

where M_Ω stands for the mass of the Ω^- baryon in the decuplet. q_α represents the momentum transfer $q_\alpha = p'_\alpha - p_\alpha$ and its square is given by $q^2 = -Q^2$ with $Q^2 > 0$. $u^\alpha(p, s)$ designates the Rarita–Schwinger spinor, carrying the momentum p and the spin component s projected along the direction of the momentum.

The multipole EM form factors can be expressed in terms of F_i in Eq. (30):

$$G_{E0}(Q^2) = \left(1 + \frac{2}{3}\tau\right)[F_1 - \tau F_2] - \frac{1}{3}\tau(1 + \tau)[F_3 - \tau F_4],$$

$$G_{E2}(Q^2) = [F_1 - \tau F_2] - \frac{1}{2}(1 + \tau)[F_3 - \tau F_4],$$

$$G_{M1}(Q^2) = \left(1 + \frac{4}{5}\tau\right)[F_1 + F_2] - \frac{2}{5}\tau(1 + \tau)[F_3 + F_4],$$

$$G_{M3}(Q^2) = [F_1 + F_2] - \frac{1}{2}(1 + \tau)[F_3 + F_4], \tag{31}$$

where $\tau = Q^2/4M_\Omega^2$. These four form factors are called, respectively, the electric or Coulomb monopole ($E0$), magnetic dipole ($M1$), electric quadrupole ($E2$), and magnetic octupole ($M3$) form factors. At $Q^2 = 0$, the values of these form factors are reduced to the charge, the magnetic dipole moment, the electric quadrupole moment, and the magnetic octupole moment, respectively:

$$e_\Omega = eG_{E0}(0),$$

$$\mu_\Omega = G_{M1}(0)\left(\frac{M_N}{M_\Omega}\right)\mu_N,$$

$$Q_\Omega = \frac{e}{M_\Omega^2}G_{E2}(0),$$

$$O_\Omega = \frac{e}{M_\Omega^3}G_{M3}(0). \tag{32}$$

Note that the electric quadrupole moment is proportional to $1/N_c$ and the magnetic octupole moment is of order $1/N_c^2$. Thus, $M3$ vanishes when we consider the corrections to order $1/N_c$.

In the Breit frame, i.e., $\boldsymbol{p'} = -\boldsymbol{p} = \boldsymbol{q}/2$, the electric and magnetic parts of the multipole form factors are related to the temporal and spatial components of the EM current, respectively:

$$G_{E0}(Q^2) = \int \frac{d\Omega_q}{4\pi}\langle\Omega^-(p', 3/2)|J^0(0)|\Omega^-(p, 3/2)\rangle,$$

$$G_{E2}(Q^2) = -\int d\Omega_q\sqrt{\frac{5}{4\pi}}\frac{3}{2}\frac{1}{\tau}\langle\Omega^-(p', 3/2)|Y_{20}^*(\Omega_q)J^0(0)|\Omega^-(p, 3/2)\rangle,$$

$$G_{M1}(Q^2) = \frac{3M_\Omega}{4\pi}\int \frac{d\Omega_q}{iQ^2}q^i\epsilon^{ik3}\langle\Omega^-(p', 3/2)|J^k(0)|\Omega^-(p, 3/2)\rangle,$$

$$G_{M3}(Q^2) = -\frac{35M_\Omega}{8}\sqrt{\frac{5}{\pi}}\int \frac{d\Omega_q}{iQ^2\tau}q^i\epsilon^{ik3}\langle\Omega^-(p', 3/2)|\left(Y_{20}^*(\Omega_q) + \sqrt{\frac{1}{5}}Y_{00}^*(\Omega_q)\right)J^k(0)|\Omega^-(p, 3/2)\rangle. \tag{33}$$

The matrix elements of the EM current can be computed within the framework of the χQSM, which has already been done in Ref. [43], with the rotational $1/N_c$ and linear m_s corrections considered. For detailed calculations, we refer to Ref. [43]. For convenience, we compile the expressions for the EM form factors of the Ω baryon in Appendix Appendix: A.

We can derive the axial-vector form factors of the Ω^- baryon in a similar manner. Since Ω^- is an isosinglet baryon, the triplet components of the Ω^- axial-vector form factors vanish. The axial-vector current of the quark field is defined as

$$A_\mu^0 := i\psi^\dagger(x)\gamma_\mu\gamma^5\psi(x), \quad A_\mu^8(x) := i\psi^\dagger(x)\gamma_\mu\gamma^5\frac{\lambda^8}{2}\psi(x). \tag{34}$$

The matrix elements of the axial-vector currents for the Ω^- baryon can again be parametrized by four different real form factors as follows:

$$\langle \Omega^-(p', s)|A^0_\mu(0)|\Omega^-(p, s)\rangle = -\bar{u}^\alpha(p', s)\left[\gamma_\mu\left\{g^{(0)}_1(q^2)\eta_{\alpha\beta} + h^{(0)}_1(q^2)\frac{q_\alpha q_\beta}{4M^2_\Omega}\right\}\right.$$
$$\left. + \frac{q^\mu}{2M_\Omega}\left\{g^{(0)}_3(q^2)\eta_{\alpha\beta} + h^{(0)}_3(q^2)\frac{q_\alpha q_\beta}{4M^2_\Omega}\right\}\right]\gamma^5 u^\beta(p, s),$$

$$\langle \Omega^-(p', s)|A^8_\mu(0)|\Omega^-(p, s)\rangle = -\bar{u}^\alpha(p', s)\left[\gamma_\mu\left\{g^{(8)}_1(q^2)\eta_{\alpha\beta} + h^{(8)}_1(q^2)\frac{q_\alpha q_\beta}{4M^2_\Omega}\right\}\right.$$
$$\left. + \frac{q^\mu}{2M_\Omega}\left\{g^{(8)}_3(q^2)\eta_{\alpha\beta} + h^{(8)}_3(q^2)\frac{q_\alpha q_\beta}{4M^2_\Omega}\right\}\right]\frac{\gamma^5}{2}u^\beta(p, s). \quad (35)$$

Since the axial-vector form factors $g^{(0, 8)}_1$ and $g^{(0, 8)}_3$ are the most important ones among the axial-vector form factors, we will concentrate on them in the present work. Moreover, they are directly related to the strong coupling constants for the $\eta\Omega\Omega$ and $\eta'\Omega\Omega$ vertices [35]. In the Breit frame, the form factors defined in Eq. (35) are expressed in terms of the spatial parts of the axial-vector current projected by the spherical basis vectors e_n:

$$g^{(0, 8)}_1(Q^2) = -\sqrt{\frac{3}{2}}\frac{M_\Omega}{E_\Omega}\langle\Omega^-(p', 3/2)|e_1 \cdot \left(A^0(0), 2A^8(0)\right)|\Omega^-(p, 1/2)\rangle,$$

$$g^{(0, 8)}_3(Q^2) = -\frac{4M^2_\Omega}{Q^2}\left[\langle\Omega^-(p', 3/2)|e_0 \cdot \left(A^0(0), 2A^8(0)\right)|\Omega^-(p, 3/2)\rangle\right.$$
$$\left. - \sqrt{\frac{3}{2}}\frac{M_\Omega}{E_\Omega}\langle\Omega^-(p', 3/2)|e_1 \cdot \left(A^0(0), 2A^8(0)\right)|\Omega^-(p, 1/2)\rangle\right], \quad (36)$$

where E_Ω corresponds to the energy of the corresponding baryon, i.e., $E_\Omega = \sqrt{M^2_\Omega + Q^2/4}$, and the spherical unit vectors e_n are expressed in terms of the Cartesian basis vectors $e_0 = \hat{z}$, $e_1 = -(\hat{x} + i\hat{y})/\sqrt{2}$, $e_{-1} = (\hat{x} - i\hat{y})/\sqrt{2}$. The matrix elements of the projected currents $e_i \cdot \left(A^0(0), 2A^8(0)\right)$ can be computed within the framework of the χQSM. The detailed formalism can be found in Ref. [44]. We list the expressions for the EM form factors of the Ω baryon in Appendix Appendix: B.

4.   Results and discussion

We first present the results for the $E0$, $M1$, and $E2$ form factors of the Ω^- baryon, showing separately the valence- and sea-quark contributions. We already expect that the sea-quark contributions will be greatly changed by replacing the pion cloud with the kaon one. In the upper-left (right) panel of Fig. 1, we depict the numerical results for the $E0$ form factors with the pion (kaon) cloud. Since the $E0$ form factor of Ω^- at $Q^2 = 0$ should be the same as its charge as shown in Eq. (32) because of the U(1) gauge symmetry, one can see that replacing the pion cloud with the kaon one enhances the valence-quark contribution but suppresses that of the sea quark. We find similar features for the $M1$ and $E2$ form factors by observing the results presented respectively in the middle and lower panels of Fig. 1. In particular, the sea-quark contribution to the $E2$ form factor is drastically reduced when the pion cloud is replaced with the kaon cloud. As already discussed in Ref. [43], the $E2$ form factors of the baryon decuplet are in general very sensitive to the tail. This indicates that the deformation of a baryon with
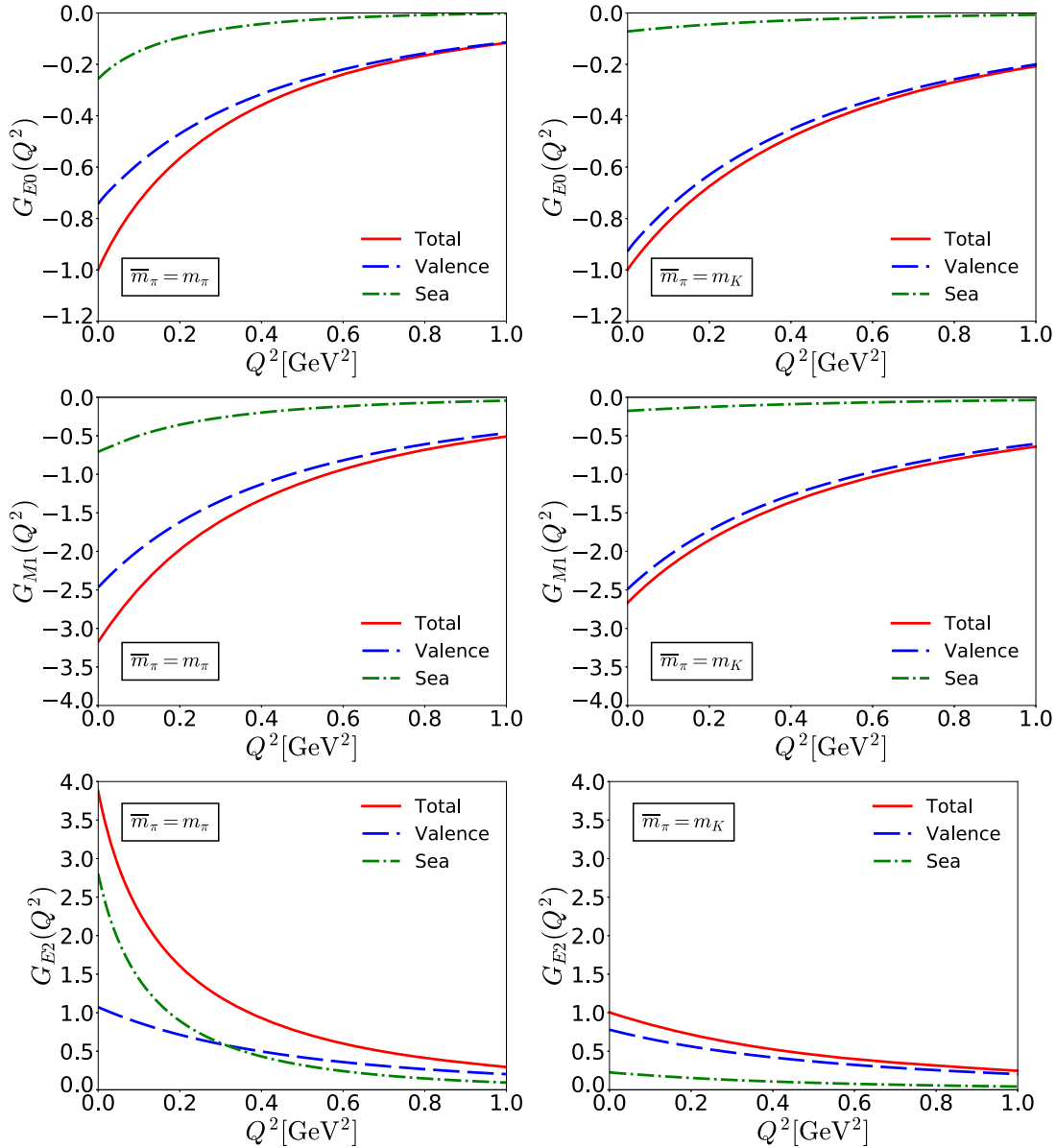
Fig. 1. Numerical results for the $E0$, $M1$, $E2$ form factors of the Ω^- baryon considering both the pion and kaon clouds. In the left panels those with the pion cloud are shown whereas in the right panels those with the kaon cloud are depicted. The dashed and dot–dashed curves exhibit the valence-quark (level-quark) and sea-quark (Dirac continuum) contributions, respectively. The solid curves show the total contributions.

spin 3/2 is governed by the sea-quark contribution or the meson clouds. On the other hand, the valence-quark contributions are not strongly influenced by changing the meson clouds.

In Fig. 2, we compare the present results for the EM form factors of Ω^- with those from lattice QCD [10]. In the upper-left panel of Fig. 2, we show the numerical results for the $E0$ form factor of Ω^-. The result with the kaon cloud falls off more slowly than that with the pion cloud and is in better agreement with the lattice data, compared with that with the pion cloud. It is well known that the lattice data on the EM form factors of the nucleon [45,46] with an unphysical pion mass fall off more slowly than the experimental data as Q^2 increases. Even if the physical pion mass is used, the lattice results for the EM form factors of the nucleon still
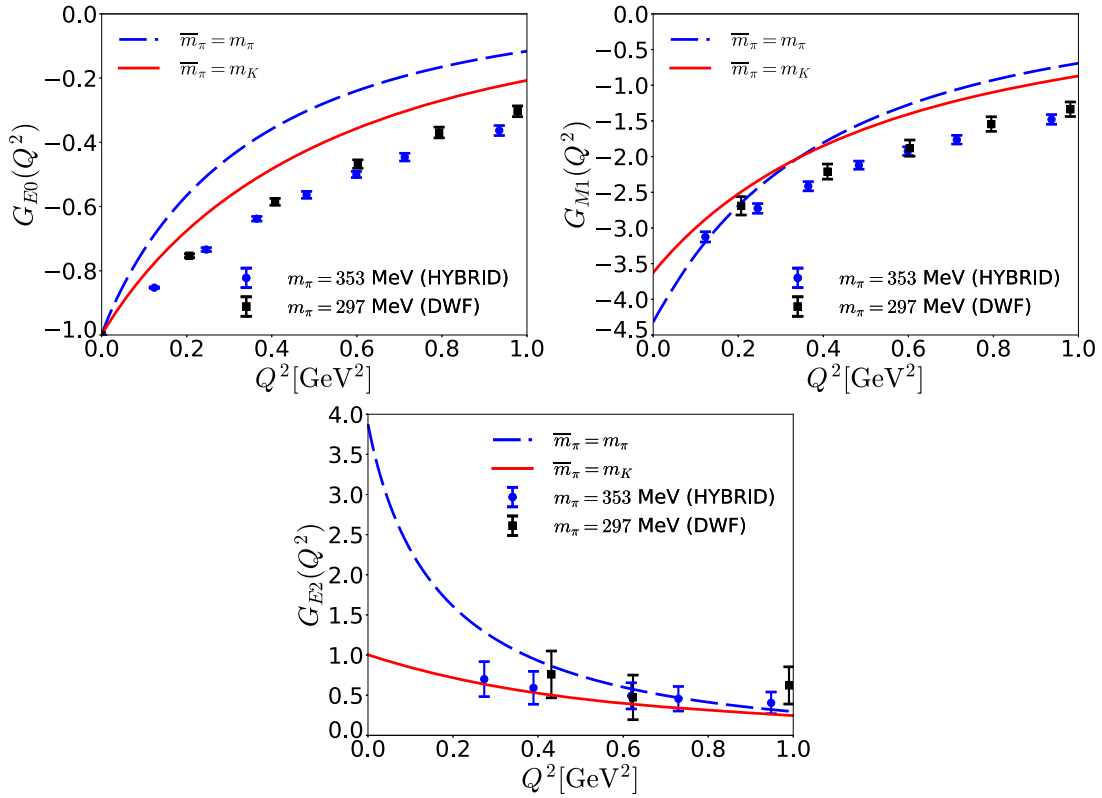
Fig. 2. Comparison of the present results for the EM form factors of the Ω^- baryon with those from lattice data. The solid curves show the results with the kaon cloud whereas the dashed ones depict those with the pion cloud. The lattice data are taken from Ref. [10]. The magnetic form factor is given in units of the soliton magneton, the reason for which is explained in the text.

overestimate the experimental data [47]. Thus, it is natural to observe that the present results for the $E0$ form factor of the Ω^- baryon fall off faster than the lattice data, as shown in the upper-left panel of Fig. 2. However, the result with the kaon cloud is markedly closer to the lattice data than that with the pion one.

In the upper-right panel of Fig. 2, we depict the results for the $M1$ form factor of Ω^-. Before we discuss them, we want to mention that the magnetic dipole moments of the SU(3) baryons are given in terms of the soliton magneton instead of the nuclear magneton. There are two reasons for doing this. Firstly, while the mass differences of the baryon octet and decuplet and even singly heavy baryons are well reproduced within the χQSM [26,40,48,49], the absolute values of these masses are always overestimated. This is a well-known problem in any chiral solitonic approaches. Secondly, the magnetic dipole moments of the baryon octet and decuplet are always underestimated by about 30%. Thus, it is theoretically consistent and empirically plausible to express the values of the magnetic dipole moments in units of the soliton magneton, which improves the theoretical results for the magnetic dipole moments in comparison with the experimental data. As shown in the upper-right panel of Fig. 2, the result for the $M1$ form factors of Ω^- with the kaon cloud is again in better agreement with the lattice data, compared with that with the pion one.

The lower panel of Fig. 2 illustrates how the kaon cloud suppresses the $E2$ form factor of Ω^-. It is remarkable that the kaon cloud reduces the magnitude of the $E2$ form factor by almost a factor of 4 and the numerical result with the kaon cloud is in far better agreement with the

Table 1. Numerical results for the electromagnetic observables in comparison with the lattice data [11]. Those for the magnetic dipole moment of the Ω^- baryon are compared with the experimental data [7].

	$\langle r^2 \rangle_E$ (fm^2)	$\mu\,(\mu_N)$	$G_{E2}(0)$
$\bar{m}_\pi = m_\pi$	0.83	-2.48	3.88
$\bar{m}_\pi = m_K$	0.51	-2.04	1.00
Exp [7]	$-$	$-2.02(5)$	$-$
LQCD [10]	0.348(52)	$-1.875(399)$	0.898(60)

Table 2. Magnetic dipole moment of the Ω^- baryon in comparison with the results from lattice QCD [50–52], the relativistic quark model [53], next-to-leading-order HBχPT [54], large N_c [55], QCD sum rules [56], the chiral quark model [57], covariant χPT [58], χPT [59], and the experimental data [7].

	$\bar{m}_\pi = m_\pi$	$\bar{m}_\pi = m_K$	[7]	[50]	[51]	[52]	[54]	[58]	[59]	[55]	[53]	[57]	[56]
$\mu_{\Omega^-}\,(\mu_N)$	-2.48	-2.04	$-2.02(5)$	$-1.73(22)$	$-1.70(7)$	$-1.93(8)$	$-1.94(22)$	-2.02	$-2.02(5)$	-1.94	-2.35	-2.13	$-1.49(45)$

Table 3. Electric quadrupole moment of the Ω^- baryon in comparison with the quark model [60], HBχPT [54], the Skyrme model [61], large N_c [62], the chiral quark model [57], and the QCD sum rules [63,64].

	$\bar{m}_\pi = m_\pi$	$\bar{m}_\pi = m_K$	[54]	[62]	[60]	[61]	[57]	[63,64]
Q_{Ω^-} (fm^2)	0.054	0.014	0.009(5)	0.027	0.028	0	0.026	0.12(4)

lattice data, compared to that with the pion cloud. As already seen in Ref. [43], the sea-quark contribution or the meson-cloud effect is dominant over that of the valence quarks. This is natural, since the $E2$ form factor measures how much the baryon with spin 3/2 is deformed from the spherical shape. This implies that the Ω^- baryon is less deformed than the Δ isobar, since it is energetically easier to create the pion cloud than the kaon one. Comparing the results with the lattice data, we observe that the numerical result with the kaon cloud is indeed in good agreement with them. On the other hand, that with the pion cloud deviates from the lattice data in smaller Q^2 regions.

Table 1 lists the numerical results for the charge radius, magnetic dipole moment, and the value of the $E2$ form factor at $Q^2 = 0$, i.e., $G_{E2}(0)$ of the Ω^- baryon. Those with the kaon cloud are prominently in better agreement with the lattice data than those with the pion cloud. In the case of the magnetic dipole moment, we also find that the result with the kaon cloud is in better agreement with the result from lattice QCD. In Tables 2 and 3, we compare the present results respectively for the magnetic dipole moment and the electric quadrupole moment of the Ω^- baryon with those obtained from other approaches. As already discussed in Ref. [43], the present numerical result for the $E2$ moment turns out to be larger than those from other works. We now can see that this discrepancy arises from the fact that only when the kaon cloud is properly considered can the $E2$ moment be correctly reproduced. This emphasizes the important role of the kaon cloud in describing the Ω^- baryon.

We now turn to the axial-vector form factors of the Ω^- baryon. Since it is an isoscalar baryon, it is not coupled to the isovector axial-vector current. So, we first consider the singlet axial-vector form factors of Ω^-. The axial-vector form factor $g_1^{(0)}$ is related to the spin content of the Ω baryon; i.e., its value at $Q^2 = 0$ has the same physical meaning as $g_A^{(0)}$ of the nucleon. The value of $g_A^{(0)}$ becomes null in the Skyrme model [65,66], whereas it acquires a small value from
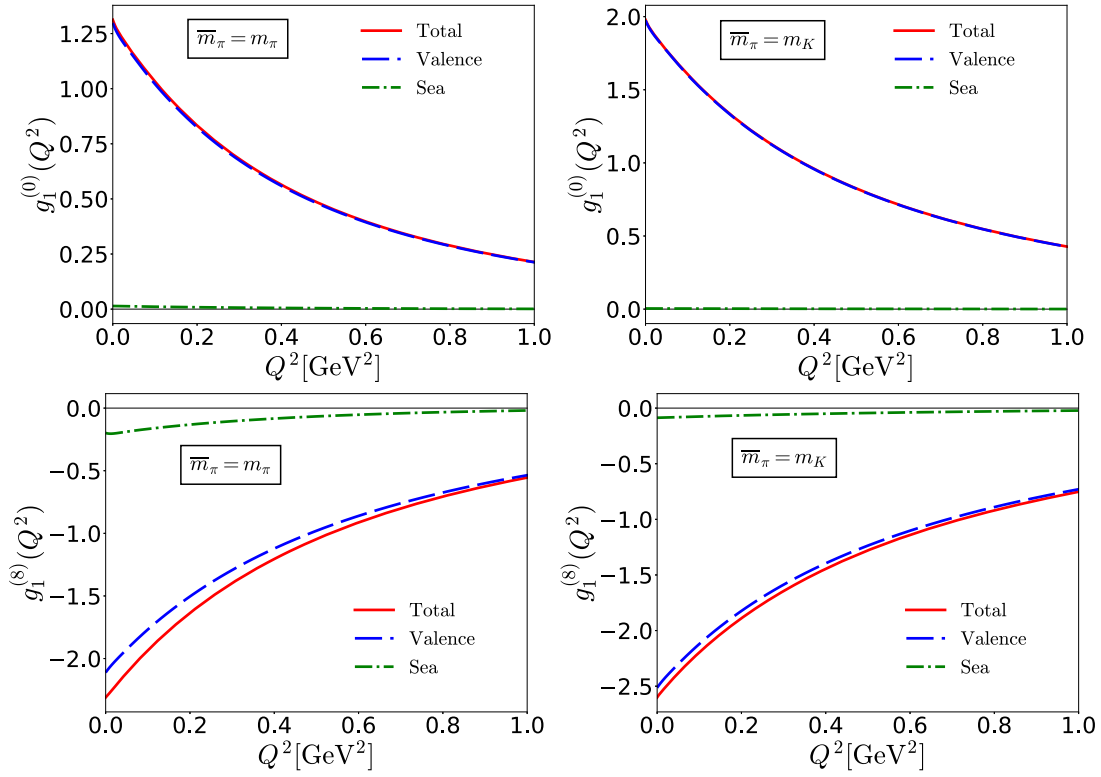
Fig. 3. Numerical results for the $g_1^{(0)}$ and $g_1^{(8)}$ axial-vector form factors of the Ω^- baryon considering both the pion and kaon clouds. In the left panels those with the pion cloud are shown whereas in the right panels those with the kaon cloud are depicted. The dashed and dot–dashed curves exhibit the valence-quark (level-quark) and sea-quark (Dirac continuum) contributions, respectively. The solid curves show the total contributions.

the rotational $1/N_c$ corrections in the χQSM [67,68]. The results from the χQSM were later improved by employing symmetry-conserving quantization [36,69]. In Ref. [69], it was shown that the kaon cloud does not greatly change the strange component of the singlet axial charge and the values of $g_A^{(0)}$, $g_A^{(3)}$, and $g_A^{(8)}$ for the nucleon were obtained respectively to be $g_A^{(0)} = 0.367$, $g_A^{(3)} = 1.176$, and $g_A^{(8)} = 0.360$. Subtle differences between these two models were discussed in great detail in Ref. [70]. Figure 3 illustrates how the valence- and sea-quark contributions are changed by the replacement of the pion cloud with the kaon one. Interestingly, the sea-quark contributions are not greatly changed by the kaon cloud. However, once the kaon cloud is considered, the valence-quark contribution enhances $g_1^{(0)}(Q^2)$ by about 40%. This can be observed clearly in the upper-left panel of Fig. 4. On the other hand, the kaon cloud increases the value of $g_1^{(8)}$ by about 10% (see Figs. 3 and 4). It is interesting to compare the present result for $g_1^{(0)}(Q^2)$ of Ω^- with that of the Δ^+ isobar. When the pion cloud is adopted, there is almost no difference between $g_1^{(0)}(Q^2)$ of the Δ^+ and Ω^- baryons, as presented in Ref. [44]. However, once we replace the pion cloud with the kaon one, the situation is drastically changed. $g_1^{(0)}$ of Ω^- is about 40% larger than that of Δ^+. This indicates that the up and down sea quarks are less likely to pop up in the Ω^- baryons, compared with the role of the strange quark in the Δ^+ baryon. So, the sea quarks inside Ω^- are less polarized. In the lower panel of Fig. 3, we depict the results for $g_1^{(8)}$. The valence-quark contribution is enhanced by about 15% whereas that of the sea quark is suppressed by about 50% when the kaon cloud is employed. Altogether, the result for $g_1^{(8)}$ is
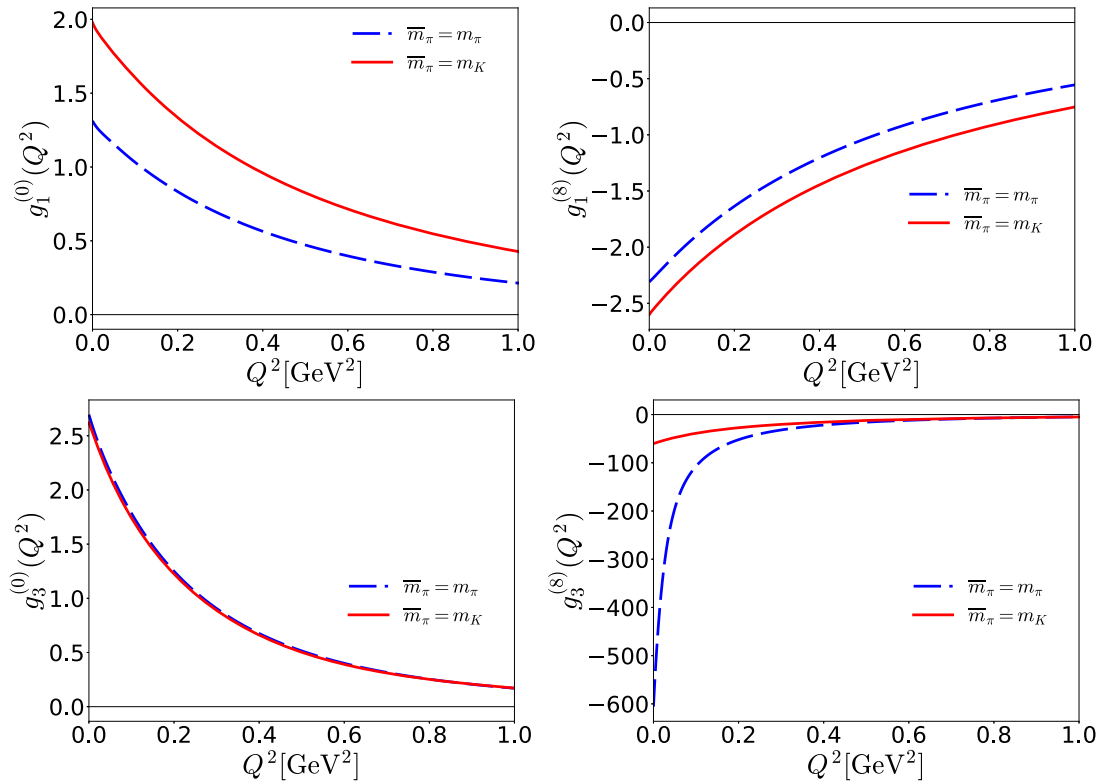
Fig. 4. Comparison of the present results for the axial-vector form factors of Ω^-. The solid curves show the results with the kaon cloud whereas the dashed ones depict those with the pion cloud.

enhanced by about 12% with the kaon cloud, as shown more clearly in the upper-right panel of Fig. 4.

In the upper panel of Fig. 5 we show the numerical results for $g_3^{(0)}$, which show that $g_3^{(0)}$ is almost unaffected by the replacement of the pion cloud with the kaon one. However, the kaon cloud notably reduces the magnitude of $g_1^{(8)}$ as shown in the lower panel of Fig. 5 by about a factor of 10. In particular, the contribution of the valence quarks is not greatly influenced by the replacement of the pion cloud with the kaon one, whereas the sea-quark contribution is tremendously lessened. This can be understood by the fact that the expression for $g_3^{(8)}$ is rather sensitive to the tail part of the soliton profile function. So far, there are no lattice data on the $g_3^{(8)}$ form factor of the Ω^- baryon. It would be very interesting if one could compare the present result with the lattice data in the near future. In Fig. 4, we compare the results for the axial-vector form factors with the kaon cloud to those with the pion one. Table 4 summarizes the values of the axial charges of the Ω^- baryon, comparing them with the lattice data [11]. With the kaon cloud, the present results for $g_1^{(0)}$ are in better agreement with the lattice data. However, we do not see any particular improvement in $g_1^{(8)}$ by replacing the pion cloud with the kaon one.

5. Summary and conclusions

In the present work, we have investigated the effects of the kaon cloud on the electromagnetic and axial-vector properties of the Ω^- baryon. We first briefly reviewed the mesonic sector, explaining how the kaonic properties can be described within the present framework. The cutoff parameters and the average value of the up and down quark masses were fixed by the pion decay constant and the pion mass, respectively. Then we were able to reproduce the kaon mass.
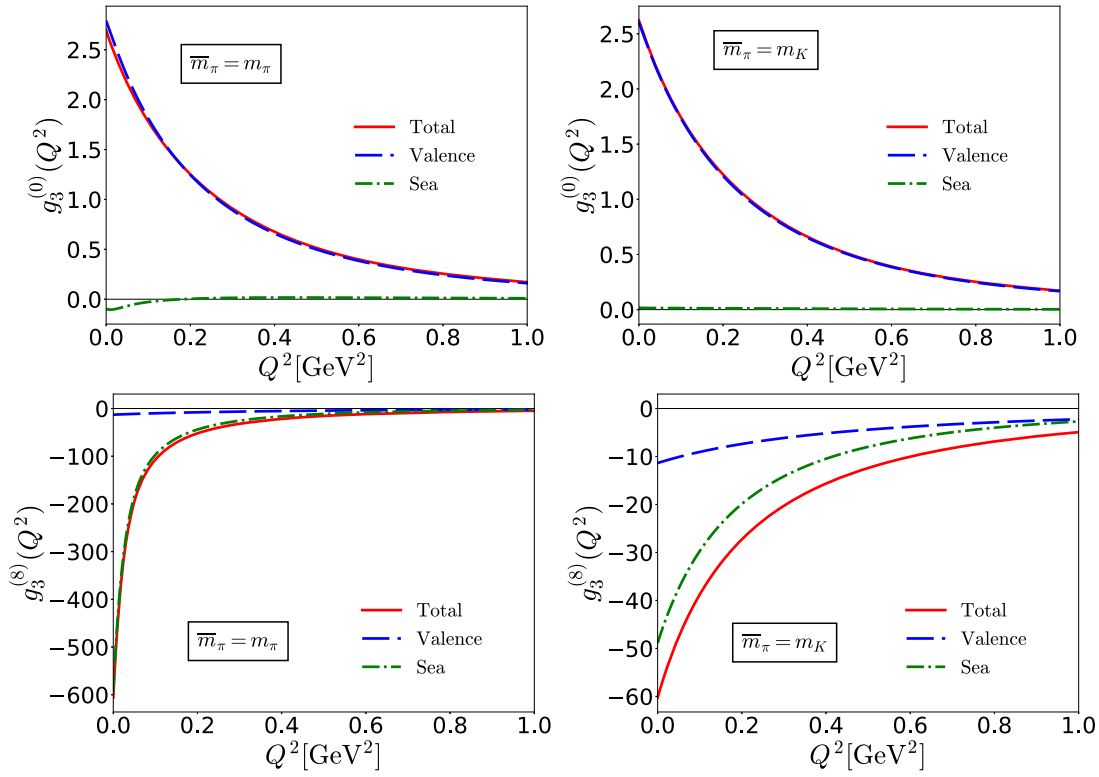
Fig. 5. Numerical results for the $g_3^{(0)}$ and $g_3^{(8)}$ axial-vector form factors of the Ω^- baryon with both the pion and kaon clouds considered. In the left panels those with the pion cloud are shown whereas in the right panels those with the kaon cloud are depicted. The dashed and dot–dashed curves exhibit the valence-quark (level-quark) and sea-quark (Dirac continuum) contributions, respectively. The solid curves show the total contributions.

Table 4. Numerical results for the axial charges $g_1^{(0,8)}$ and $g_3^{(0,8)}$ in comparison with those from lattice QCD (LQCD) [11]. Since the expressions for the octet axial-vector current $A_\mu^8(x)$ in Ref. [11] are different from the present one by $\sqrt{3}$, we have considered it for comparison.

	$g_1^{(0)}(0)$	$g_1^{(8)}(0)$	$g_3^{(0)}(0)$	$g_3^{(8)}(0)$
$\overline{m}_\pi = m_\pi$	1.313	-3.863	2.696	-605.734
$\overline{m}_\pi = m_K$	1.979	-4.296	2.619	-60.290
LQCD ($m_\pi = 213\,\mathrm{MeV}$)	2.0365 ± 0.0303	-4.0731 ± 0.0606	–	–
LQCD ($m_\pi = 256\,\mathrm{MeV}$)	1.9606 ± 0.0376	-3.9212 ± 0.0752	–	–
LQCD ($m_\pi = 302\,\mathrm{MeV}$)	2.0215 ± 0.0441	-4.0431 ± 0.0883	–	–
LQCD ($m_\pi = 373\,\mathrm{MeV}$)	1.9044 ± 0.0439	-3.8087 ± 0.0877	–	–
LQCD ($m_\pi = 432\,\mathrm{MeV}$)	1.9562 ± 0.0457	-3.9125 ± 0.0915	–	–

The average quark mass of the up and down quarks inside the one-body Dirac Hamiltonian produces the asymptotic pion Yukawa tail of the solitonic profile function and this proper behavior of the Yukawa tail is called the pion tail. Since the Ω^- baryon consists of triple strange valence quarks, the kaon cloud is required. Thus, we changed the value of the average quark mass in such a way that the proper kaon Yukawa tail was produced. While this is theoretically somewhat inconsistent, it improves phenomenologically the description of the Ω^- baryon. As long as we consider only the Ω^- baryon, this kaon tail provides an even more plausible theoreti-

cal ground than the pion one. Employing the kaon cloud, we computed the electromagnetic and axial-vector form factors of the Ω^- baryon. In the case of the electromagnetic form factors, the kaon cloud mainly suppresses the sea-quark contributions whereas those of the valence quarks are not greatly affected. When the kaon cloud is considered, the present results for the $E0$, $M1$, and $E2$ form factors are in better agreement with the lattice data in comparison with those obtained by the pion cloud. The results for the electric quadrupole moment are also in better agreement with those from other works. We then calculated the axial-vector form factors of the Ω^- baryon and discussed the differences between the results with the kaon cloud and those with the pion one. The value of the singlet axial-vector form factor $g_1^{(0)}$ is increased by about 40%, whereas the octet one $g_1^{(8)}$ is enhanced by about 12%. While the $g_3^{(0)}$ form factor is almost kept intact, $g_3^{(8)}$ is drastically reduced by about a factor of 10 when the pion cloud is replaced with the kaon one.

Since the strange valence quark is deeply related to the kaon cloud, it is of great importance to examine how the kaon cloud affects all other hyperons with double strange valence quarks. In particular, because the singlet axial charges $g_1^{(0)}(0)$ provide information on the spin content of these baryons, one has to consider the effects of the kaon cloud. A corresponding investigation is underway.

Appendix: A. Electromagnetic form factors

In Appendix Appendix: A, we compile all the expressions for the EM form factors of the Ω baryon within the framework of the χQSM:

$$G_{E0}(Q^2) = e_\Omega \int d^3r\, j_0(Q|r|) \left[\frac{1}{24}\mathcal{B}(r) + \frac{5}{8I_1}\mathcal{I}_1(r) + \frac{1}{4I_2}\mathcal{I}_2(r) \right], \tag{A1}$$

where the densities of the electric form factor are written explicitly as

$$\frac{1}{N_c}\mathcal{B}(r) = \langle \text{val}|r\rangle\langle r|\text{val}\rangle - \frac{1}{2}\sum_n \text{sign}(E_n)\langle n|r\rangle\langle r|n\rangle,$$

$$\frac{6}{N_c}\mathcal{I}_1(r) = \sum_{n\neq\text{val}} \frac{1}{E_n - E_\text{val}} \langle \text{val}|r\rangle\tau\langle r|n\rangle \cdot \langle n|\tau|\text{val}\rangle + \frac{1}{2}\sum_{n,m} \langle n|\tau|m\rangle \cdot \langle m|r\rangle\tau\langle r|n\rangle \mathcal{R}_3(E_n, E_m),$$

$$\frac{4}{N_c}\mathcal{I}_2(r) = \sum_{n^0} \frac{1}{E_{n^0} - E_\text{val}} \langle n^0|\text{val}\rangle\langle \text{val}|r\rangle\langle r|n^0\rangle + \sum_{n,m^0} \langle n|m^0\rangle\langle m^0|r\rangle\langle r|n\rangle \mathcal{R}_3(E_n, E_{m^0}). \tag{A2}$$

The expression for the magnetic dipole form factor of the Ω baryon is written as

$$G_{M1}(Q^2) = -\frac{1}{8}e_\Omega\frac{M_\Omega}{Q} \int d^3r \frac{j_1(Q|r|)}{|r|} \left[\left(\mathcal{Q}_0(r) + \frac{1}{I_1}\mathcal{Q}_1(r) \right) + \frac{1}{2}\frac{1}{I_1}\mathcal{X}_1(r) + \frac{1}{2}\frac{1}{I_2}\mathcal{X}_2(r) \right], \tag{A3}$$

where the corresponding densities are expressed explicitly as follows:

$$
\frac{1}{N_c}\mathcal{Q}_0(\boldsymbol{r}) = \langle\mathrm{val}|\boldsymbol{r}\rangle\gamma^5\{\boldsymbol{r}\times\boldsymbol{\sigma}\}\cdot\boldsymbol{\tau}\langle\boldsymbol{r}|\mathrm{val}\rangle + \sum_n \mathcal{R}_1(E_n)\langle n|\boldsymbol{r}\rangle\gamma^5\{\boldsymbol{r}\times\boldsymbol{\sigma}\}\cdot\boldsymbol{\tau}\langle\boldsymbol{r}|n\rangle,
$$

$$
\frac{2}{N_c}\mathcal{Q}_1(\boldsymbol{r}) = i\sum_{n\neq\mathrm{val}}\frac{\mathrm{sign}(E_n)}{E_n - E_{\mathrm{val}}}\langle n|\boldsymbol{r}\rangle\gamma^5[\{\boldsymbol{r}\times\boldsymbol{\sigma}\}\times\boldsymbol{\tau}]\langle\boldsymbol{r}|\mathrm{val}\rangle\cdot\langle\mathrm{val}|\boldsymbol{\tau}|n\rangle
$$

$$
+ i\frac{1}{2}\sum_{n,m}\mathcal{R}_4(E_n,E_m)\langle m|\boldsymbol{r}\rangle\gamma^5[\{\boldsymbol{r}\times\boldsymbol{\sigma}\}\times\boldsymbol{\tau}]\langle\boldsymbol{r}|n\rangle\cdot\langle m|\boldsymbol{\tau}|n\rangle,
$$

$$
\frac{1}{N_c}\mathcal{X}_1(\boldsymbol{r}) = \sum_{n\neq\mathrm{val}}\frac{1}{E_n - E_{\mathrm{val}}}\langle\mathrm{val}|\boldsymbol{r}\rangle\gamma^5\{\boldsymbol{r}\times\boldsymbol{\sigma}\}\langle\boldsymbol{r}|\mathrm{val}\rangle\cdot\langle n|\boldsymbol{\tau}|\mathrm{val}\rangle
$$

$$
+ \frac{1}{2}\sum_{n,m}\mathcal{R}_5(E_n,E_m)\langle n|\boldsymbol{r}\rangle\gamma^5\{\boldsymbol{r}\times\boldsymbol{\sigma}\}\langle\boldsymbol{r}|m\rangle\cdot\langle m|\boldsymbol{\tau}|n\rangle,
$$

$$
\frac{1}{N_c}\mathcal{X}_2(\boldsymbol{r}) = \sum_{n^0}\frac{1}{E_{n^0} - E_{\mathrm{val}}}\langle\mathrm{val}|\boldsymbol{r}\rangle\gamma^5\{\boldsymbol{r}\times\boldsymbol{\sigma}\}\cdot\boldsymbol{\tau}\langle\boldsymbol{r}|n^0\rangle\langle n^0|\mathrm{val}\rangle
$$

$$
+ \sum_{n^0,m}\mathcal{R}_5(E_m,E_{n^0})\langle m|\boldsymbol{r}\rangle\gamma^5\{\boldsymbol{r}\times\boldsymbol{\sigma}\}\cdot\boldsymbol{\tau}\langle\boldsymbol{r}|n^0\rangle\langle n^0|m\rangle. \tag{A4}
$$

The expression for the electric quadrupole form factor of Ω baryon is obtained as

$$
G_{E2}(Q^2) = 3\sqrt{5}e_\Omega M_\Omega^2\int d^3r\frac{j_2(Q|\boldsymbol{r}|)}{Q^2}\left[\frac{1}{I_2}\mathcal{I}_{E2}(\boldsymbol{r})\right], \tag{A5}
$$

where the densities of the electric quadrupole form factors are given as

$$
(-\sqrt{10})\frac{2}{N_c}\mathcal{I}_{1E2}(\boldsymbol{r}) = \sum_{n\neq\mathrm{val}}\frac{1}{E_n - E_{\mathrm{val}}}\langle\mathrm{val}|\boldsymbol{\tau}|n\rangle\cdot\langle n|\boldsymbol{r}\rangle\{\sqrt{4\pi}\,Y_2\otimes\tau_1\}_1\langle\boldsymbol{r}|\mathrm{val}\rangle
$$

$$
+ \frac{1}{2}\sum_{n,m}\mathcal{R}_3(E_n,E_m)\langle n|\boldsymbol{\tau}|m\rangle\cdot\langle m|\boldsymbol{r}\rangle\{\sqrt{4\pi}\,Y_2\otimes\tau_1\}_1\langle\boldsymbol{r}|n\rangle, \tag{A6}
$$

where $|\mathrm{val}\rangle$ and $|n\rangle$ denote the states of the valence and sea quarks with the corresponding eigenenergies E_{val} and E_n of the single-quark Hamiltonian $h(U_c)$, respectively [26]. The regularization functions $\mathcal{R}_1(E_n,E_m),\ldots,\mathcal{R}_5(E_n,E_m)$ will be given at the end of Appendix, Appendix: B.

Appendix: B. Axial-vector form factors

The axial-vector form factors of Ω^- in the χQSM are expressed as

$$g_1^{(0)}(Q^2) = \frac{2N_c M_\Omega}{9E_\Omega} \int d^3r \left[j_0(Q|\mathbf{r}|)\frac{\mathcal{B}_0(\mathbf{r})}{I_1} - j_2(Q|\mathbf{r}|)\frac{\mathcal{B}_2(\mathbf{r})}{I_1} \right],$$

$$g_3^{(0)}(Q^2) = -\frac{8N_c M_\Omega^2}{9E_\Omega Q^2} \int d^3r \left[j_0(Q|\mathbf{r}|)(E_\Omega - M_\Omega)\frac{\mathcal{B}_0(\mathbf{r})}{I_1} + j_2(Q|\mathbf{r}|)(2E_\Omega + M_\Omega)\frac{\mathcal{B}_2(\mathbf{r})}{I_1} \right],$$

$$g_1^{(8)}(Q^2) = \frac{\sqrt{3}N_c M_\Omega}{24E_\Omega} \int d^3r \left[j_0(Q|\mathbf{r}|)\left\{ 2\mathcal{A}_0(\mathbf{r}) - \frac{\mathcal{B}_0(\mathbf{r})}{I_1} - \frac{\mathcal{C}_0(\mathbf{r})}{I_2} - \frac{i\mathcal{D}_0(\mathbf{r})}{I_1} \right\} \right.$$
$$\left. - j_2(Q|\mathbf{r}|)\left\{ 2\mathcal{A}_2(\mathbf{r}) - \frac{\mathcal{B}_2(\mathbf{r})}{I_1} - \frac{\mathcal{C}_2(\mathbf{r})}{I_2} - \frac{i\mathcal{D}_2(\mathbf{r})}{I_1} \right\} \right],$$

$$g_3^{(8)}(Q^2) = -\frac{\sqrt{3}N_c M_\Omega^2}{6E_\Omega Q^2} \int d^3r \left[j_0(Q|\mathbf{r}|)(E_\Omega - M_\Omega)\left\{ 2\mathcal{A}_0(\mathbf{r}) - \frac{\mathcal{B}_0(\mathbf{r})}{I_1} - \frac{\mathcal{C}_0(\mathbf{r})}{I_2} - \frac{i\mathcal{D}_0(\mathbf{r})}{I_1} \right\} \right.$$
$$\left. + j_2(Q|\mathbf{r}|)(2E_\Omega + M_\Omega)\left\{ 2\mathcal{A}_2(\mathbf{r}) - \frac{\mathcal{B}_2(\mathbf{r})}{I_1} - \frac{\mathcal{C}_2(\mathbf{r})}{I_2} - \frac{i\mathcal{D}_2(\mathbf{r})}{I_1} \right\} \right], \tag{B1}$$

where the components $\mathcal{A}_0(\mathbf{r}), \ldots, \mathcal{D}_0(\mathbf{r})$ are written as

$$\mathcal{A}_0(\mathbf{r}) = \langle \mathrm{val}|\mathbf{r}\rangle \boldsymbol{\sigma} \cdot \boldsymbol{\tau} \langle \mathbf{r}|\mathrm{val}\rangle + \sum_n \langle n|\mathbf{r}\rangle \boldsymbol{\sigma} \cdot \boldsymbol{\tau} \langle \mathbf{r}|n\rangle \mathcal{R}_1(E_n),$$

$$\mathcal{B}_0(\mathbf{r}) = \sum_{n\neq\mathrm{val}} \frac{1}{E_\mathrm{val} - E_n} \langle \mathrm{val}|\mathbf{r}\rangle \boldsymbol{\sigma} \langle \mathbf{r}|n\rangle \cdot \langle n|\boldsymbol{\tau}|\mathrm{val}\rangle - \frac{1}{2} \sum_{n,m} \langle n|\mathbf{r}\rangle \boldsymbol{\sigma} \langle \mathbf{r}|m\rangle \cdot \langle m|\boldsymbol{\tau}|n\rangle \mathcal{R}_5(E_n, E_m),$$

$$\mathcal{C}_0(\mathbf{r}) = \sum_{n_0\neq\mathrm{val}} \frac{1}{E_\mathrm{val} - E_{n_0}} \langle \mathrm{val}|\mathbf{r}\rangle \boldsymbol{\sigma} \cdot \boldsymbol{\tau} \langle \mathbf{r}|n_0\rangle \langle n_0|\mathrm{val}\rangle - \sum_{n,m_0} \langle n|\mathbf{r}\rangle \boldsymbol{\sigma} \cdot \boldsymbol{\tau} \langle \mathbf{r}|m_0\rangle \langle m_0|n\rangle \mathcal{R}_5(E_n, E_{m_0}),$$

$$\mathcal{D}_0(\mathbf{r}) = \sum_{n\neq\mathrm{val}} \frac{\mathrm{sgn}(E_n)}{E_\mathrm{val} - E_n} \langle \mathrm{val}|\mathbf{r}\rangle (\boldsymbol{\sigma} \times \boldsymbol{\tau}) \langle \mathbf{r}|n\rangle \cdot \langle n|\boldsymbol{\tau}|\mathrm{val}\rangle$$
$$+ \frac{1}{2} \sum_{n,m} \langle n|\mathbf{r}\rangle \boldsymbol{\sigma} \times \boldsymbol{\tau} \langle \mathbf{r}|m\rangle \cdot \langle m|\boldsymbol{\tau}|n\rangle \mathcal{R}_4(E_n, E_m). \tag{B2}$$

$\mathcal{A}_2(\boldsymbol{r}), \ldots, \mathcal{D}_2(\boldsymbol{r})$ in Eq. (B1) are given by

$$\mathcal{A}_2(\boldsymbol{r}) = \langle \text{val}|\boldsymbol{r}\rangle \left\{ \sqrt{2\pi} \, Y_2 \otimes \sigma_1 \right\}_1 \cdot \boldsymbol{\tau}\langle \boldsymbol{r}|\text{val}\rangle + \sum_n \langle n|\boldsymbol{r}\rangle \left\{ \sqrt{2\pi} \, Y_2 \otimes \sigma_1 \right\}_1 \cdot \boldsymbol{\tau}\langle \boldsymbol{r}|n\rangle \mathcal{R}_1(E_n),$$

$$\mathcal{B}_2(\boldsymbol{r}) = \sum_{n \neq \text{val}} \frac{1}{E_{\text{val}} - E_n} \langle \text{val}|\boldsymbol{r}\rangle \left\{ \sqrt{2\pi} \, Y_2 \otimes \sigma_1 \right\}_1 \langle \boldsymbol{r}|n\rangle \cdot \langle n|\boldsymbol{\tau}|\text{val}\rangle$$

$$- \frac{1}{2} \sum_{n,m} \langle n|\boldsymbol{r}\rangle \left\{ \sqrt{2\pi} \, Y_2 \otimes \sigma_1 \right\}_1 \langle \boldsymbol{r}|m\rangle \cdot \langle m|\boldsymbol{\tau}|n\rangle \mathcal{R}_5(E_n, E_m),$$

$$\mathcal{C}_2(\boldsymbol{r}) = \sum_{n_0 \neq \text{val}} \frac{1}{E_{\text{val}} - E_{n_0}} \langle \text{val}|\boldsymbol{r}\rangle \left\{ \sqrt{2\pi} \, Y_2 \otimes \sigma_1 \right\}_1 \cdot \boldsymbol{\tau}\langle \boldsymbol{r}|n_0\rangle \langle n_0|\text{val}\rangle$$

$$- \sum_{n,m_0} \langle n|\boldsymbol{r}\rangle \left\{ \sqrt{2\pi} \, Y_2 \otimes \sigma_1 \right\}_1 \cdot \boldsymbol{\tau}\langle \boldsymbol{r}|m_0\rangle \langle m_0|n\rangle \mathcal{R}_5(E_n, E_{m_0}),$$

$$\mathcal{D}_2(\boldsymbol{r}) = \sum_{n \neq \text{val}} \frac{\text{sgn}(E_n)}{E_{\text{val}} - E_n} \langle \text{val}|\boldsymbol{r}\rangle \left\{ \sqrt{2\pi} \, Y_2 \otimes \sigma_1 \right\}_1 \times \boldsymbol{\tau}\langle \boldsymbol{r}|n\rangle \cdot \langle n|\boldsymbol{\tau}|\text{val}\rangle$$

$$+ \frac{1}{2} \sum_{n,m} \langle n|\boldsymbol{r}\rangle \left\{ \sqrt{2\pi} \, Y_2 \otimes \sigma_1 \right\}_1 \times \boldsymbol{\tau}\langle \boldsymbol{r}|m\rangle \cdot \langle m|\boldsymbol{\tau}|n\rangle \mathcal{R}_4(E_n, E_m). \tag{B3}$$

The regularization functions are defined by

$$\mathcal{R}_1(E_n) = -\frac{1}{2\sqrt{\pi}} E_n \int_0^\infty \phi(u) \frac{du}{u} e^{-uE_n^2},$$

$$\mathcal{R}_2(E_n, E_m) = \frac{1}{2\sqrt{\pi}} \int_0^\infty \phi(u) \frac{du}{\sqrt{u}} \frac{E_m e^{-uE_m^2} - E_n e^{-uE_n^2}}{E_n - E_m},$$

$$\mathcal{R}_3(E_n, E_m) = \frac{1}{2\sqrt{\pi}} \int_0^\infty \phi(u) \frac{du}{\sqrt{u}} \left[\frac{e^{-uE_m^2} - e^{-uE_n^2}}{u(E_n^2 - E_m^2)} - \frac{E_m e^{-uE_m^2} + E_n e^{-uE_n^2}}{E_n + E_m} \right],$$

$$\mathcal{R}_4(E_n, E_m) = \frac{1}{2\pi} \int_0^\infty \phi(u) du \int_0^1 d\alpha \, e^{-uE_n^2(1-\alpha) - uE_m^2 \alpha} \frac{E_n(1-\alpha) - \alpha E_m}{\sqrt{\alpha(1-\alpha)}},$$

$$\mathcal{R}_5(E_n, E_m) = \frac{\text{sign}(E_n) - \text{sign}(E_m)}{2(E_n - E_m)}. \tag{B4}$$

References

[1] V. E. Barnes et al. Phys. Rev. Lett. **12**, 204 (1964).
[2] S. F. Biagi et al. Z. Phys. C **31**, 33 (1986).
[3] D. Aston et al. Phys. Lett. B **194**, 579 (1987).
[4] D. Aston et al. Phys. Lett. B **215**, 799 (1988).
[5] J. Yelton et al. [Belle Collaboration] Phys. Rev. Lett. **121**, 052003 (2018).
[6] S. Jia et al. [Belle Collaboration], Phys. Rev. D **100**, 032006 (2019).
[7] P. A. Zyla et al. [Particle Data Group], Prog. Theor. Exp. Phys. **2020**, 083C01 (2020).
[8] S. Acharya et al. [ALICE Collaboration], Nature **588**, 232 (2020).
[9] T. Iritani et al. [HAL QCD Collaboration], Phys. Lett. B **792**, 284 (2019).
[10] C. Alexandrou, T. Korzec, G. Koutsou, J. W. Negele, and Y. Proestos, Phys. Rev. D **82**, 034504 (2010).
[11] C. Alexandrou, K. Hadjiyiannakou, and C. Kallidonis, Phys. Rev. D **94**, 034502 (2016).
[12] D. R. Yennie, M. M. Levy, and D. G. Ravenhall, Rev. Mod.Phys. **29**, 144 (1957).
[13] W. R. Frazer and J. R. Fulco, Phys. Rev. Lett. **2**, 365 (1959).
[14] W. R. Frazer and J. R. Fulco, Phys. Rev. **117**, 1603 (1960).

[15] W. R. Frazer and J. R. Fulco, Phys. Rev. **117**, 1609 (1960).
[16] G. Cohen-Tannoudji, V. V. Ilyin, and L. L. Jenkovszky, Lett. Nuovo Cimento **5S2**, 957 (1972) [Lett. Nuovo Cimento **5**, 957 (1972)].
[17] A. A. Anselm and V. N. Gribov, Phys. Lett. B **40**, 487 (1972).
[18] G. S. Adkins and C. R. Nappi, Nucl. Phys. B **233**, 109 (1984).
[19] L. L. Frankfurt and M. I. Strikman, Phys. Rept. **160**, 235 (1988).
[20] H.-W. Hammer, Eur. Phys. J. A **28**, 49 (2006).
[21] U. G. Meissner, AIP Conf. Proc. **904**, 142 (2007).
[22] L. Jenkovszky, I. Szanyi, and C. I. Tan, Eur. Phys. J. A **54**, 116 (2018).
[23] E. Witten, Nucl. Phys. B **160**, 57 (1979).
[24] D. Diakonov, V. Y. Petrov, and P. V. Pobylitsa, Nucl. Phys. B **306**, 809 (1988).
[25] D. Diakonov, arXiv:hep-ph/9802298 [Search inSPIRE].
[26] C. Christov, A. Blotz, H.-Ch. Kim, P. Pobylitsa, T. Watabe, T. Meissner, E. Ruiz Arriola, and K. Goeke, Prog. Part. Nucl. Phys. **37**, 91 (1996).
[27] H.-Ch. Kim, A. Blotz, M. V. Polyakov, and K. Goeke, Phys. Rev. D **53**, 4013 (1996).
[28] E. Witten, Nucl. Phys. B **223**, 422 (1983).
[29] S. Jain and S. R. Wadia, Nucl. Phys. B **258**, 713 (1985).
[30] T. Watabe, H.-CH. Kim, and K. Goeke, arXiv:hep-ph/9507318 [Search inSPIRE].
[31] H.-Ch. Kim, T. Watabe, and K. Goeke, Nucl. Phys. A **616**, 606 (1997).
[32] A. Silva, H.-Ch. Kim, and K. Goeke, Phys. Rev. D **65**, 014016 (2002); **66**, 039902 (2002) [erratum].
[33] A. Silva, H.-Ch. Kim, and K. Goeke, Eur. Phys. J. A **22**, 481 (2004).
[34] A. Silva, H.-Ch. Kim, D. Urbano, and K. Goeke, Phys. Rev. D **74**, 054011 (2006).
[35] G. S. Yang and H.-Ch. Kim, Phys. Lett. B **785**, 434 (2018).
[36] M. Praszalowicz, T. Watabe, and K. Goeke, Nucl. Phys. A **647**, 49 (1999).
[37] M. Jaminon, G. Ripka, and P. Stassart, Nucl. Phys. A **504**, 733 (1989).
[38] M. Jaminon, R. Mendez Galain, G. Ripka, and P. Stassart, Nucl. Phys. A **537**, 418 (1992).
[39] L. F. Abbott, Acta Phys. Polon. B **13**, 33 (1982).
[40] A. Blotz, D. Diakonov, K. Goeke, N. W. Park, V. Petrov, and P. V. Pobylitsa, Nucl. Phys. A **555**, 765 (1993).
[41] C. G. Callan Jr, K. Hornbostel, and I. R. Klebanov, Phys. Lett. B **202**, 269 (1988).
[42] H. Yabu and K. Ando, Nucl. Phys. B **301**, 601 (1988).
[43] J.-Y. Kim and H.-Ch. Kim, Eur. Phys. J. C **79**, 570 (2019).
[44] Y. S. Jun, J. M. Suh, and H.-Ch. Kim, Phys. Rev. D **102**, 054011 (2020).
[45] S. Capitani, M. Della Morte, D. Djukanovic, G. von Hippel, J. Hua, B. Jäger, B. Knippschild, H. B. Meyer, T. D. Rae, and H. Wittig, Phys. Rev. D **92**, 054511 (2015).
[46] M. T. Hansen and S. R. Sharpe, Phys. Rev. D **93**, 096006 (2016); **96**, 039901 (2017) [erratum].
[47] C. Alexandrou, M. Constantinou, K. Hadjiyiannakou, K. Jansen, C. Kallidonis, G. Koutsou, and A. Vaquero Aviles-Casco, Phys. Rev. D **96**, 034503 (2017).
[48] J. Y. Kim, H.-Ch. Kim, and G. S. Yang, Phys. Rev. D **98**, 054004 (2018).
[49] J. Y. Kim and H.-Ch. Kim, Prog. Theor. Exp. Phys. **2020**, 043D03 (2020).
[50] D. B. Leinweber, T. Draper, and R. M. Woloshyn, Phys. Rev. D **46**, 3067 (1992).
[51] S. Boinepalli, D. B. Leinweber, P. J. Moran, A. G. Williams, J. M. Zanotti, and J. B. Zhang, Phys. Rev. D **80**, 054505 (2009).
[52] C. Aubin, K. Orginos, V. Pascalutsa, and M. Vanderhaeghen, Phys. Rev. D **79**, 051502 (2009).
[53] F. Schlumpf, Phys. Rev. D **48**, 4478 (1993).
[54] M. N. Butler, M. J. Savage, and R. P. Springer, Phys. Rev. D **49**, 3459 (1994).
[55] M. A. Luty, J. March-Russell, and M. J. White, Phys. Rev. D **51**, 2332 (1995).
[56] F. X. Lee, Phys. Rev. D **57**, 1801 (1998).
[57] G. Wagner, A. J. Buchmann, and A. Faessler, J. Phys. G **26**, 267 (2000).
[58] L. S. Geng, J. Martin Camalich, and M. J. Vicente Vacas, Phys. Rev. D **80**, 034027 (2009).
[59] H. S. Li, Z. W. Liu, X. L. Chen, W. Z. Deng, and S. L. Zhu, Phys. Rev. D **95**, 076001 (2017).
[60] M. I. Krivoruchenko and M. M. Giannini, Phys. Rev. D **43**, 3763 (1991).
[61] Y. S. Oh, Mod. Phys. Lett. A **10**, 1027 (1995).
[62] A. J. Buchmann and R. F. Lebed, Phys. Rev. D **67**, 016002 (2003).
[63] K. Azizi, Eur. Phys. J. C **61**, 311 (2009).
[64] T. M. Aliev, K. Azizi, and M. Savci, Phys. Lett. B **681**, 240 (2009).

[65] S. J. Brodsky, J. R. Ellis, and M. Karliner, Phys. Lett. B **206**, 309 (1988).
[66] J. R. Ellis and M. Karliner, Phys. Lett. B **213**, 73 (1988).
[67] A. Blotz, M. Praszalowicz, and K. Goeke, Phys. Lett. B **317**, 195 (1993).
[68] A. Blotz, M. Praszalowicz, and K. Goeke, Phys. Rev. D **53**, 485 (1996).
[69] A. Silva, H.-Ch. Kim, D. Urbano, and K. Goeke, Phys. Rev. D **72**, 094011 (2005).
[70] M. Wakamatsu, Prog. Theor. Phys. **95**, 143 (1996)